Numerical Simulation of Direct Contact Membrane Desalination (DCMD): II

Isam Janajreh
Masdar Institute of Science and Technology
ijanajreh@masdar.ac.ae

Dana Suwwan
Masdar Institute of Science and Technology
dsuwwan@masdar.ac.ae

Abstract

With the help of ANSYS Fluent, we were able to study the steady state performance of low energy direct contact membrane distillation (DCMD). The DCMD setup consists of two uniform fluid flows separated by a thin PVDF membrane of hydrophobic nature. The flow is governed by the Navier-Stokes flow, coupled with the energy equation in conjugate heat transfer formulation. The performance of the setup is influenced greatly by the membrane characteristics including permeability, thickness, pore size, and conductivity. The mechanism lies within the fact that local temperature difference is created and hence causes a driving pressure gradient responsible for phase change of the feed at the surface, transporting the vapor through the pores and condensing it at the permeate side where it is flushed out. During this analysis, mass and heat transfer modules were examined with varying flow properties and membrane parameters. As functions, temperature polarization, mass flux, and heat flux were studied under different flow velocities and parametric configurations. Results showed a good agreement with the published theoretical work. In view of these results, a sensitivity study to the flow rates is performed to gain better insight into the temperature polarization; heat flux, including convective, conductive; and the associated latent heat, as well as in understanding the effect on the process metrics and yield.

Introduction

Direct contact membrane distillation (DCMD) is gaining more popularity because of the required low-grade energy compared to other technologies such as MSF or RO [1].The advantages of the DCMD lie in its simplicity, utilization of a low-grade temperature difference, and the potential of achieving near 100% rejection of dissolved solids [2]. In addition, membrane processes can be modular and flexible for scale up, keeping the advantage that separation is occurring under mild conditions [3]. Another benefit lies in the variable membrane properties, which can be adjusted. A review on the design of membrane distillation can be found elsewhere [4, 5] which includes, in addition to the DCMD, air gap membrane distillation, vacuum membrane distillation, and sweeping gas membrane distillation, as illustrated in Figure 1 below.
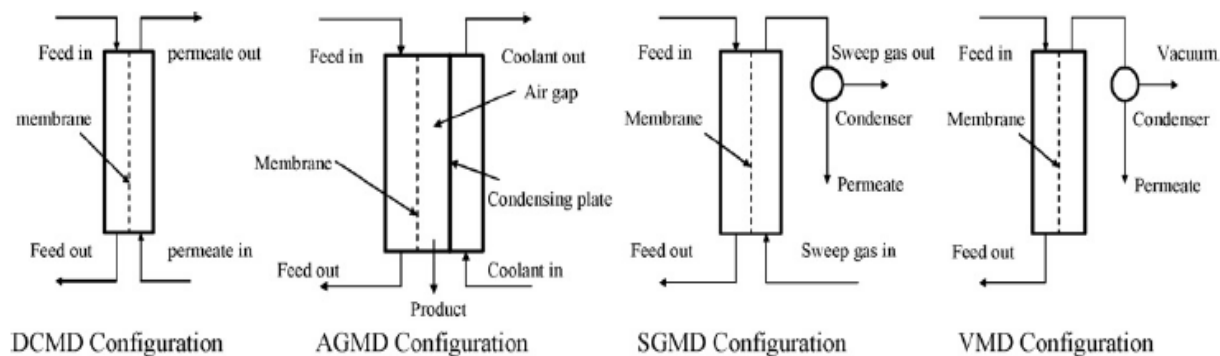
Figure 1. Different DCMD configurations

The DCMD incorporates a phase-change at the feed side, transmembrane flux towards the permeate side, and condensation at the permeate side [4]. It is different from the classical multistage flash, multi-effect distillation, vapor compression, freezing, and humidification/dehumidification, solar stills electrodialysis, reverse osmosis, and common membrane distillation [1]. Many of these common techniques require the consumption of large amounts of fossil fuels to power a dedicated desalination plant or indirectly through cogeneration. DCMD is a well-known water production application providing separation and purification.

The anatomy of the DCMD consists of two flows with different temperatures and species separated by a hydrophobic membrane, which is in direct contact to the flows. The feed flow is typically the flow with higher temperature than the permeate flow. The temperature difference between the two flows across the contacting membrane surface creates a difference in the potential vapor partial pressure. This difference drives the transport of vapor mass and energy transfer from the hotter feed side to the cooler permeate side.

This work aims at obtaining fundamental understanding of the DCMD setup and its pronounced parameters through a high fidelity flow simulation and sensitivity study. DCMD's pure water productivity was presented in several macroscopic models. Several empirical and semi-empirical models were also proposed in [3]. Recently, a model that includes the temperature polarization for a flat DCMD was proposed that was helpful in understanding the transmembrane flux mechanism.

Hui Yu et al. conducted a numerical study considering the transmembrane heat and mass fluxes of the DCMD membrane in a hollow fiber tube [6]. They used similar conjugate heat transfer models and studied the influence of the mass flow and length of the membrane but with less emphasis on the combined width, length, velocity effect. Others utilized less accurate semi-empirical correlation, constant mass flux coefficient, single side of the flow, or stack of thermal resistances to arrive to the prediction of the driving process temperature distribution [2, 7-10]. Zhang et al. [7, 11] are among the pioneers who modeled the DCMD as conjugate heat considering the sandwiched membrane and its surrounding fluids, yet without consideration of any phase change. The mean spatial temperature was also estimated by the work Fane et al. using the boundary layer analogy [12, 13]. However, due to strong coupling of the two flow sides and the semi-conductive membrane and its transmembrane

flux, these empirical models fall short of providing reliable and comprehensive flow information to the two-dimensional temperature distribution and thereby to the special heat transfer coefficients [4, 14]. These findings considered both parallel and counter flow arrangement. Results of CFD simulations and experimental work were compared in terms of mass fluxes and temperature distributions. They found that temperature polarization decreases upstream and then increases downstream. The local heat fluxes increased and then decreased with the flow direction. Nusselt numbers were also reported to be highest at the entrance due to a thin thermal boundary layer and prior to the developing flow. Most importantly, the thermal efficiency, defined as the heat carried by the transmembrane flux to the total heat, was studied, and it was found that higher velocities does, in fact, enhance the transmembrane mass flux but decreases efficiency due to heat loss on the permeate side resulting from conduction.

On the other hand, a high-fidelity analysis and rather complicated fluid dynamics modeling, combined with Ergun model for pressure drop and Knudson-diffusion for transmembrane flux, was introduced by Carfi et al. [15] for modeling the DCMD. The complexity of this model, however, hindered its practicality.

Therefore, only limited literature on the high-fidelity CFD modeling of the DCMD exists today. This work is intended to enrich this literature gap by considering a comprehensive arrangement of the flow in two-dimensional laminar Navier-Stokes flow coupled with the energy conservation for the membrane in a conjugate heat transfer. This model is equally applied to parallel (or counterflow) channels as well as axisymmetric of two concentric cylindrical flows separated by the membrane. Such a model can be used as a conceptual design tool for innovative design and development in the emerging field of DCMD.

Mathematical Modelling

The mathematical modeling technique is built on our previous work, where the flow regimes were studied, that is, parallel and counter configuration, alongside with temperature effects. Therefore, this work will undergo the same steps of theoretical modeling and formulation as the past work in [14].

A schematic of the DCMD in horizontal configuration is illustrated in Figure 2 below. Overall, an aqueous hot feed (hot channel) enters the top side (outer cylinder in axisymmetric) of the membrane, while the permeate enters the bottom cold side of the membrane (inner cylinder axisymmetric). Evaporation of the feed first occurs at the top/outer membrane surface in the form of pure water, and vapor is then transported within the membrane towards the bottom surface; finally, this vapor condensates on that surface as pure permeate [17]. The performance of the DCMD depends on the temperature of the feed/permeate flows, temperature and pressures and physical membrane characteristics, permeability, conductivity, pore size and distribution, and thickness.
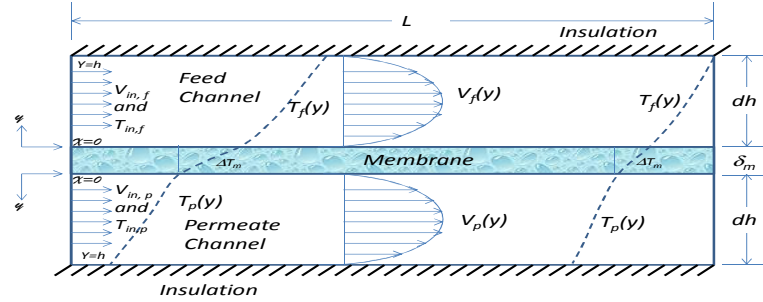
Figure 2. Schematic diagram of parallel-flow DCMD

For modeling purposes, we have assumed two-dimensional model following the Cartesian coordinates along the x and perpendicular to y directions as illustrated in Figure 2 above. The incoming velocity profiles will be considered as uniform and steady parallel flows at fixed velocity and temperature values.

Governing Equations

For the consideration steady state heated flow process, the mass and x and y Navier-Stokes (momentum) conservation are given in equations 1, 2a, and 2b, respectively.

$$\frac{\partial(\rho u)}{\partial x} + \frac{\partial(\rho v)}{\partial y} = 0 \tag{1}$$

$$u\frac{\partial(\rho u)}{\partial x} + v\frac{\partial(\rho u)}{\partial y} = -\frac{\partial P}{\partial x} + \mu\left(\frac{\partial^2 u}{\partial x^2} + \frac{\partial^2 u}{\partial y^2}\right) \tag{2a}$$

$$u\frac{\partial(\rho v)}{\partial x} + v\frac{\partial(\rho v)}{\partial y} = -\frac{\partial P}{\partial y} + \mu\left(\frac{\partial^2 v}{\partial x^2} + \frac{\partial^2 v}{\partial y^2}\right) + \rho g_y \tag{2b}$$

where $\rho\left(\frac{kg}{m3}\right), u\left(\frac{m}{s}\right), v\left(\frac{m}{s}\right), P(pa),$ and μ (pa. s) are the density, velocity in x, velocity in y, pressure and dynamic viscosity, respectively.

The scalar energy equation is also given by

$$u\frac{\partial(\rho C p T)}{\partial x} + v\frac{\partial(\rho C p T)}{\partial y} = k\left(\frac{\partial^2 T}{\partial x^2} + \frac{\partial^2 T}{\partial y^2}\right) + S_h \tag{3}$$

where $Cp\left(\frac{W}{kg.k}\right), T$ (k), and $k\left(\frac{w}{m.k}\right)$ are the specific heat, temperature, u velocity in x, v velocity in y, and k is the thermal conductivity, respectively.

S_h signifies the sink/source heat that is attributed to the latent heat of evaporation at both the feed and permeate membrane surface, respectively. It can be defined as the following work of Yu et al. as

$$S_h = \begin{cases} \frac{q_{md}}{\delta_y} \cdot \frac{y_{mo}}{y_{mi}} \; for \; y = y_{mi} \\ -\frac{q_{md}}{\delta_y} for \; y = y_{mi} \\ 0 \; otherwise \end{cases} \tag{4}$$

where the q_{md} is the membrane's feed side latent heat flux, y is the vertical distance, and the subscripts *mo* and *mi* signifies the locations of the top and bottom membrane surfaces, respectively. The S_h also holds the heat boundary conditions attributed to the flow and implicitly applied to the membrane surface.

Mass Transfer Module

In the DCMD process, evaluating the transport of mass constitutes the process productivity. Due to the temperature gradient, a driving pressure force is created which is responsible for the mass transfer across the membrane [3]. The general form of the mass flux is illustrated by Chen and Greenlee [3, 1], which is written as

$$J'' = c_m \left(P_{mf}^{sat} - P_{mp}^{sat} \right) \tag{5}$$

where c_m, P_{mf}^{sat}, and P_{mp}^{sat} are the intrinsic mass membrane coefficient, saturated pressure of water on the feed and permeate membrane's surface, respectively. The beauty of the above equation is for a given pressure-temperature relation the mass flux temperature dependency can be inferred such that

$$J'' = c_m \frac{d}{dT} \left(P_{mf}^{sat} - P_{mp}^{sat} \right) * (T_{mf} - T_{mp}) \tag{6}$$

The pressure temperature relation is tabulated in steam tables according to Antoine equation [12], which follows a monotonic form within the operational desalination temperature range. This equation is written as

$$P_{pure}^{sat} = \exp \left(23.238 - \frac{3841}{T_m - 45} \right), i \in \{f, p\} \tag{7}$$

This equation is adjusted for none pure saline or wastewater as shown in our previous work [14].

$$P_i^{sat}(x, T) = x_w a_w P_{i\,(pure)}^{sat} \; , i \in \{f, p\} \tag{8}$$

Where x_w, a_w are the mole fraction of the water in saline solution and the water activity in NaCl solutions, respectively. The temperature is expressed in Kelvin degree (K), and the pressures are given in Pascals (Pa). The water activity in NaCl solutions is estimated using correlation of Khayet [4] and Lowson [2] as

$$a_w = 1 - 0.5x_{NaCl} - 10x_{NaCl}^2 \tag{9}$$

where x_{NaCl} is the mole fraction of NaCl in the brine solution. Therefore, an increase in temperature will definitely lead to an increase in the transmembrane mass flux. This can be achieved either by operating at higher feed temperature condition or by targeting a higher temperature distribution along the membrane.

The mass coefficient is obtained from the simulation following either Knudson-diffusion, molecular diffusion, Poiseuille flow, or Monte Carlo simulation as reported by Ding et al. [18], Bui et al [19] and Imdakum and Mussarra [20].

This work uses a suitable combination between Knudson and Poiseuille models as was presented by Chen et al. [4] and is described as

$$c_m = c_k + c_p = 1.064 \ \alpha(T) \frac{\varepsilon \, r}{\tau \, \delta_m} \sqrt{\frac{M_w}{R \, T_{mt}}} + 0.125 \ \beta(T) \frac{\varepsilon \, r^2}{\tau \, \delta_m} \tag{10}$$

where $\alpha(T)$, and $\beta(T)$ are Knudsen diffusion model and Poiseuille flow model contributions, respectively. M_w is the molar mass of the water in (kg/mol), T_{mt} is the mean membrane temperature (C), R is the gas constant, P_m is the mean pressure, δ_m is the thickness of the membrane, η_v is the gas vicosity, r is the pores radius, ε is the porosity of the membrane, and τ is the tortuosity factor, which can be estimated for hydrophobic membrane by Iversen et al. [21], such as

$$\tau = \frac{1}{\varepsilon} \tag{11}$$

The transmembrane heat flux is described by the latent heat flux and conduction through the membrane. The former is written as

$$q_m = j''. \Delta H_m \tag{12}$$

where ΔH_m is the latent heat of the transmembrane fluid that permeated. The conduction is described by the Nusselt number such that

$$Nu = \frac{h.d}{k} \ or \ \frac{q.d}{k(T_b - T_m)} \tag{13}$$

where h, d, and k are the heat transfer coefficient, characteristic length and thermal conductivity. The q and is the heat flux and T is the local temperature where the subscripts b and m signify the bulk and the membrane, respectively.

Heat Transfer Module

The heat transfer in DCMD process can be described following three steps: heat transfer through the feed boundary layer, heat transfer through membrane, and heat transfer through the permeate boundary layer [17]. The total heat flux for the membrane is either due to the convection through the feed membrane surface, the convection through the permeate

membrane surface, or a combination between the conduction (Q_m) and latten heat of evaporation through the membrane. The conduction across the membrane material is in part due to the bulk membrane material conduction (Q_c) and the other is due to the vapor-filled pores(Q_v). The total membrane heat flux can be described as

$$Q_m = Q_c + Q_v \tag{14}$$

The transmembrane heat flux is written as

$$q_m = j''.\Delta H_m \tag{15}$$

where ΔH_m is the latent heat of the transmembrane flux of the fluid, according to Termpiayakul et al. [16]. This enthalpy can be fitted from the enthalpy data of saturated water vapor and liquid according to the following equation:

$$H_{m,i} = 1.7535\, T_{m,i} + 2024.3 \qquad i \in \{f, p\} \tag{16}$$

Hence, the conduction is expressed as
$$Q_{m,i} = \frac{k_m}{\delta_m}(T_{m,f} - T_{m,p}) \text{ with } K_m = (1-\varepsilon)K_b + \varepsilon K_V \tag{17}$$

Where km is the membrane conduction coefficients, T is the temperature and f and p signify the feed and permeate respectively. The K_m is the total membrane conductivity which volume weighted average of the bulk conductivity K_b and is the vapor conductivity K_V which can be estimated from the work of Chen and Ho [3].

The convective heat transfer coefficient can be described by the Nusselt number such that

$$Nu = \frac{h.d}{k} \ or \ \frac{q.d}{k(T_b - T_m)} \tag{18}$$

where h, d, and k are the convective heat transfer coefficient, characteristic length and thermal conductivity. The q above is the heat flux and T is the local temperature where the subscripts b and m signify the bulk and the membrane, respectively.

Parameters Affecting the DCMD Performance

DCMD Thermal Efficiency (η)

This metric is governed by the fraction of the heat used as latent heat of evaporation instead of the lost conduction fraction. This efficiency can be written as

$$\eta = j''.\Delta H_m / q_f \tag{19}$$

Where $q_f = j''.\Delta H_m + K_m(T_{mf} - T_{mp})/\delta_m \tag{20}$

Therefore, low membrane conductivity is desirable to increase the thermal efficiency. Dividing by the latent heat enthalpy (ΔH_m) defines the "equivalence" conductive mass flux (j''_{keq}) and hence the efficiency can be rewritten as

$$\eta = j''/(j'' + j''_{keq}) \qquad (21)$$

Equation 21 states another definition to the membrane desalination/filtration efficiency; it is the ratio of the transmembrane flux to that of the total theoretical mass flux when ignoring any lower grade heat losses, such as frictional or radiative heat.

Temperature Polarization (θ)

It measures the ratio of boundary layer resistance over the total heat transfer resistance and is expressed as

$$\theta = \frac{T_{m,f} - T_{m,p}}{T_{b,f} - T_{b,p}} \qquad (22)$$

where the subscripts m, b, f, p signify the membrane, bulk, feed flow, and permeate flow, respectively. For small θ (≤ 0.2), the DCMD is considered heat transfer limited meaning the module design is poor. For larger θ value (≥ 0.6), the DCMD enters the mass transfer limitation that is hindered because of the low membrane permeability [16]. The mathematical and CFD models are applied to determine the mass flux, heat flux, temperature polarization, and membrane coefficient for the parallel flow.

Flow Properties and Boundary Conditions

The geometry of the problem admits both 2-D and axisymmetric configurations, while only the 2-D is adopted in this work. The baseline geometry consisted of 21cm length by 0.1cm width of each channel. The membrane is sandwiched between the two channels with a 0.130 mm thickness. The flow is considered parallel flow, entering at nominal Reynolds number of 500 and inlet feed temperature of 40°C and 25°C for the permeate. A quadrilateral mesh type is used for the whole geometry, feed channel, permeate channel and the membrane. A boundary layer mesh is used at the membrane surface targeting y+ value of one unit. It progressively and smoothly expanded towards the center channel. The mesh size is 2,100x64 and 2,100x8 for the membrane. Material properties of each of the membrane, salt feed water, and permeate fresh water are summarized in Table 1. Initially, the property of the membrane is evaluated using a void-solid weighted average according to the following equation:

$$\emptyset_m = (1 - \varepsilon)\emptyset_o + \varepsilon\emptyset_v \qquad (23)$$

where $\emptyset$ is the equivalent permeable membrane property and the subscripts o and ϑ signify the core membrane material, typically polyvindeline fluoride or polyvinyl alcohol with cellulose reinforcements/enhancements, and the vapor that occupies the membrane pores.

Table 1. Properties of the of membrane and flow materials

Material	Density (kg/m^3)	Specific heat (J/kg.k)	Conductivity (w/m.k)	Viscosity (Pas)
PVDF [23]	1175	1325	0.2622	-
Vapor	0.554	2014	0.0261	-
Membrane	302.2	1896.9	0.0662	-
Saline sea water* [24]	1013.2	4064.8	0.642	5.86E-4
Pure water** [25]	995.2	4182.1	0.613	8.38E-4

* At 3.5% salinity and 323 K
**At 303K

Results and Discussion

Temperature Field

Results of the temperature profile are depicted in Figure 3 and compare favorably to Chen et al. [17]. A considerable influence exists of flow velocity on temperature distribution at the membrane surface, and this difference grows larger as the velocity is increased/doubled; it became more pronounced when the velocity is quadrupled as depicted in Figure 3a. The difference in temperature is maintained until the flow exits. It is, however. not easy to state the optimal velocity values as both the one-sided bulk and membrane surface temperatures decrease asymptotically. The shorter residence time for the flow to cool down at the feed side, or to heat up at the permeate side however delays the reduction at higher velocities. These results agree with those obtained by Chen et al. [17], as shown in Figure 3b. It is worth mentioning that the mean membrane temperature is almost constant and nearly identical for the parallel flow in the DCMD model at the three velocity values. As the permeate velocity can be controlled independently and can be kept constant, there is some interest in investigating this effect on the resulted mass flux. The membrane and bulk temperature line plot is depicted in Figure 3c, and it shows that the temperature across the membrane decreases as the velocity of the permeate remains fixed. Thus, one anticipates lower performance for inferior permeate feed velocity flow.
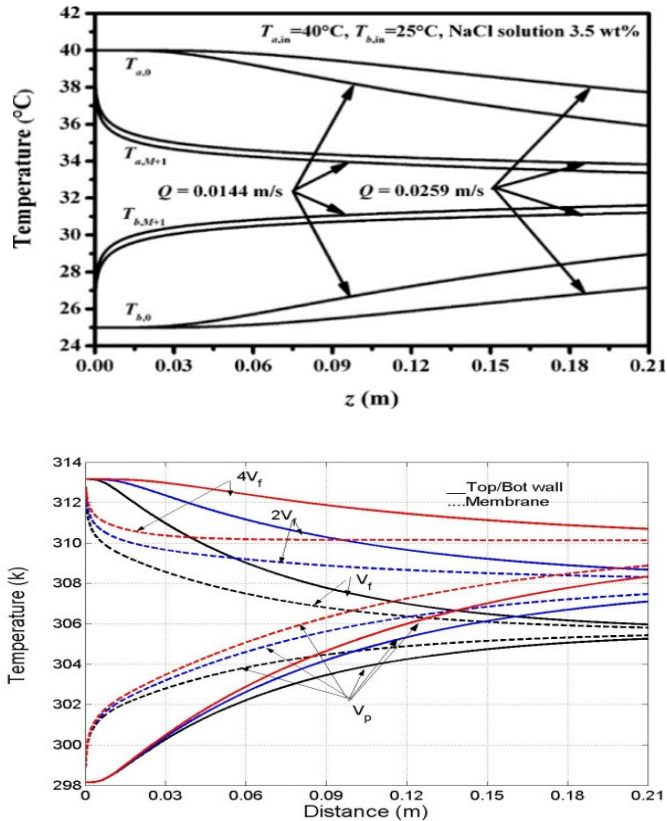
Figure 3. Temperature profiles correspond to different mass flow (inlet velocity) for parallel flow in which the feed is entering at 40° C and the permeate is at 25° C

Nusselt Number

It is depicted in Figure 4 and shows a asymptotic decreasing trend similar to the temperature. Nusselt values of the permeate side dominate initially and exceed twice the value of the feed side. The difference, however, decreases and come closer at midstream, and it nearly converges near the exit at the downstream, particularly for low inlet velocities. The equal channel velocities exhibit more spread, while for fixed permeate velocity the Nusselt values are more converged. The low values of Nusselt suggest both convection and conduction are in the same order of magnitude and slightly in the favor of convection heat transfer. These obtained values are characteristic of laminar flow and are comparable to those obtained by Hui et al.
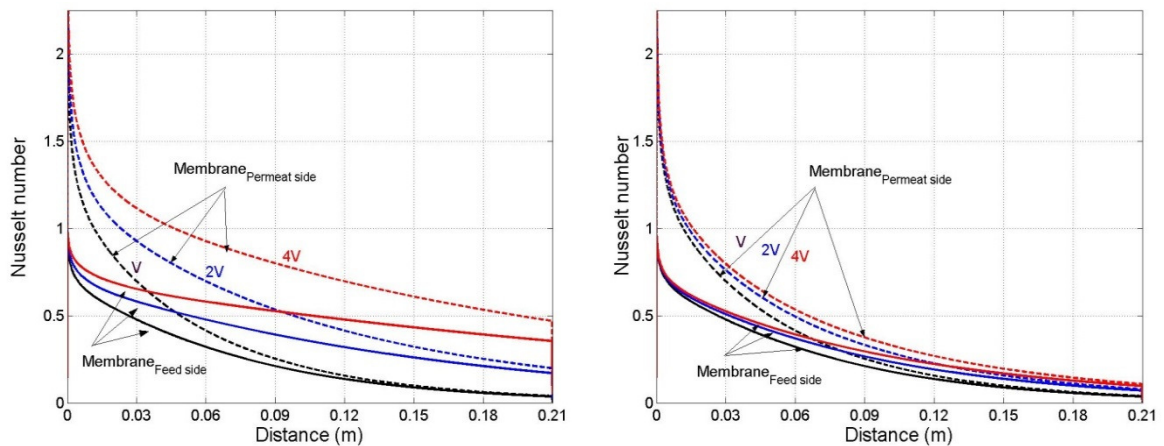
Figure 4. Nusselt number of the feed and permeate membrane surfaces at different velocity values, left at equal velocities right at fixed permeate velocity

Temperature Polarization (θ)

Additional to the thermal boundary resistance, temperature polarization provides the operational range of the parallel configuration. An asymptotic decreasing trend occurs quickly at lower velocity values. It appears that higher velocity resulted in extended mass limitation range and reaching nearly 1/10th of the channel length before it descends to the favorable range (0.6-0.2). The lower velocity appears to descend to the normal range faster and remaining to operate within the favorable range. Keeping the permeate at lower velocity value while increasing the feed velocity caused an extended mass limitation in the entry region but averaged a higher and favorable θ.
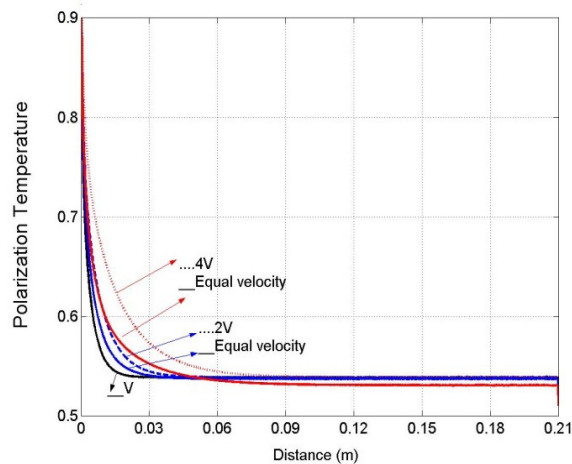

Figure 5. Temperature polarization

Mass Flux (j")

Max flux is directly affected by the incremental increase of velocity, temperature, change of configuration, and membrane characteristics. The distributed local and accumulative mass flux for the equal two-sided velocity values are depicted in Figure 6a, and those at constant permeate velocity are depicted in Figure 6b. It is clearly show that as the velocity increases the flux also increases. It tends to reach asymptotic value at low velocity while it is delayed and not reached at higher velocity. This implies that the length/velocity combination, in addition to other system properties (membrane, channel height, inlet temperature etc.), is less tuned for higher velocity than lower velocity. This is also observed at constant permeate velocity as depicted in Figure 6b, which shows the mass flux is opted to reach faster the asymptotic plateau because of the lower permeate velocity. For the current membrane property and configuration, a maximum is 5.76 kg /m^2.hr, whereas for the same high velocity of feed and lower value permeate, the total flux is 4.05 kg /m^2.hr. These values corresponding to their velocity values are summarized in Table 2.

Table 2. Summary of mass flux at the corresponding velocities

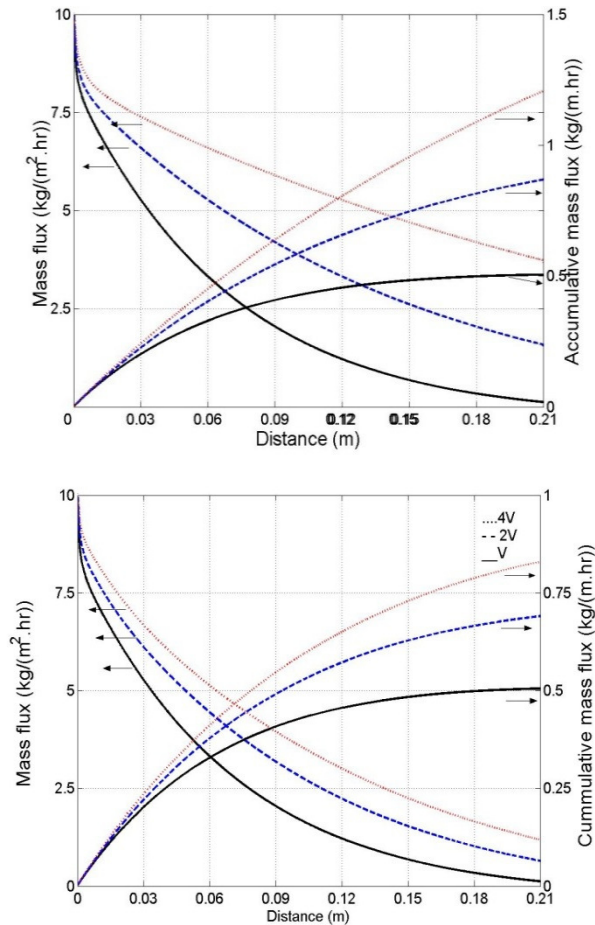| Feed Re* / velocity (m/s)	Permeate Re* / velocity (m/s)	Accumulative mass flux (kg/m^2.hr)
20 / 0.01 m/s	20 / 0.01 m/s	2.38
40 / 0.02 m/s	40 / 0.02 m/s	3.57
40 / 0.02 m/s	40 / 0.02 m/s	5.76
40 / 0.02 m/s	20 / 0.01 m/s	3.24
40 / 0.02 m/s	20 / 0.01 m/s	4.05

* Re is based on channel height of 1mm

Figure 6. Incremental and accumulative mass flux at both equal feed
and permeate velocity (top) and at fixed permeate velocity (bottom)

Heat Flux and Thermal Efficiency (η)

The heat flux and temperature difference across the membrane is depicted in Figure 7.
Higher heat is injected to the membrane at higher velocity and a similar trend is observed for
the temperature difference. This difference is indicative of the conductive heat, which is also
equal to the same convective heat flux for zero transmembrane flux. The latent heat
associated with the transmembrane flux in DMC is typically very low compared to the
conductive flux in which the former is the effective absorbed heat and the latter is considered
as conduction loss. This defines the efficiency of the DMC system, which is the ratio of the
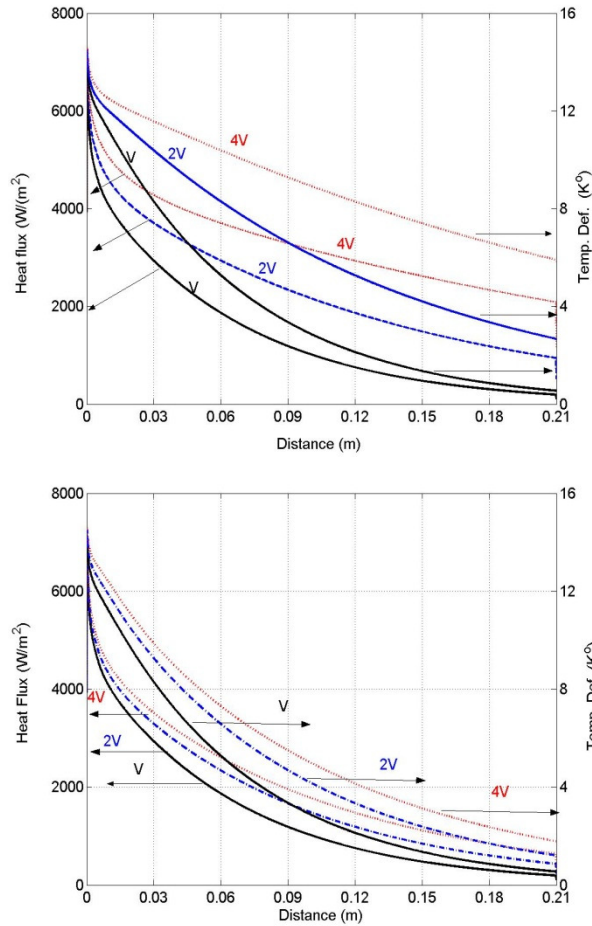latent heat to that of the total convective heat.

Figure 7. Heat flux and temperature difference across the membrane at both
equal feed and permeate (top) and fixed permeate (bottom) velocity

Figure 8 indicates efficiency of the DCMD. It reveals a very low efficiency, which
constitutes the current and main drawback of the process. Interestingly, the fixed feed
resulted in higher efficiency at double and quadruple feed velocity. Nevertheless, there is
more room to improve efficiency by 5- or even 10-fold by combining optimal flow condition
and membrane characteristics. This includes optimal flow velocity and inlet temperature,
optimal channel height, and upper and lower surface temperatures. As for the membrane
parameters, optimal porosity, tortuosity, membrane thickness, and very low conductivity are
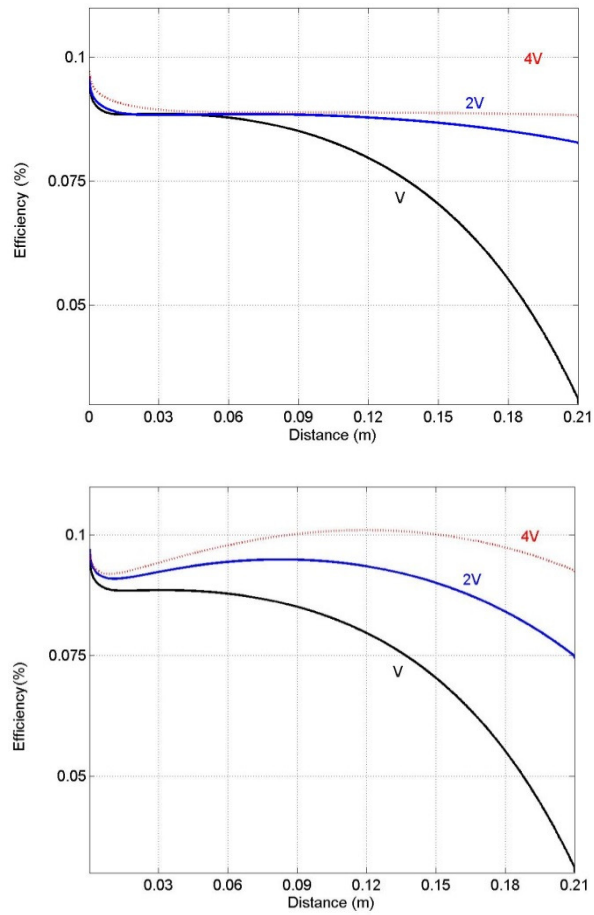the chief parameters to enhance the DCMD process metrics.

Figure 8. The DCMD evaluated efficiency (top) equal feed and permeate (bottom) fixed permeate velocity
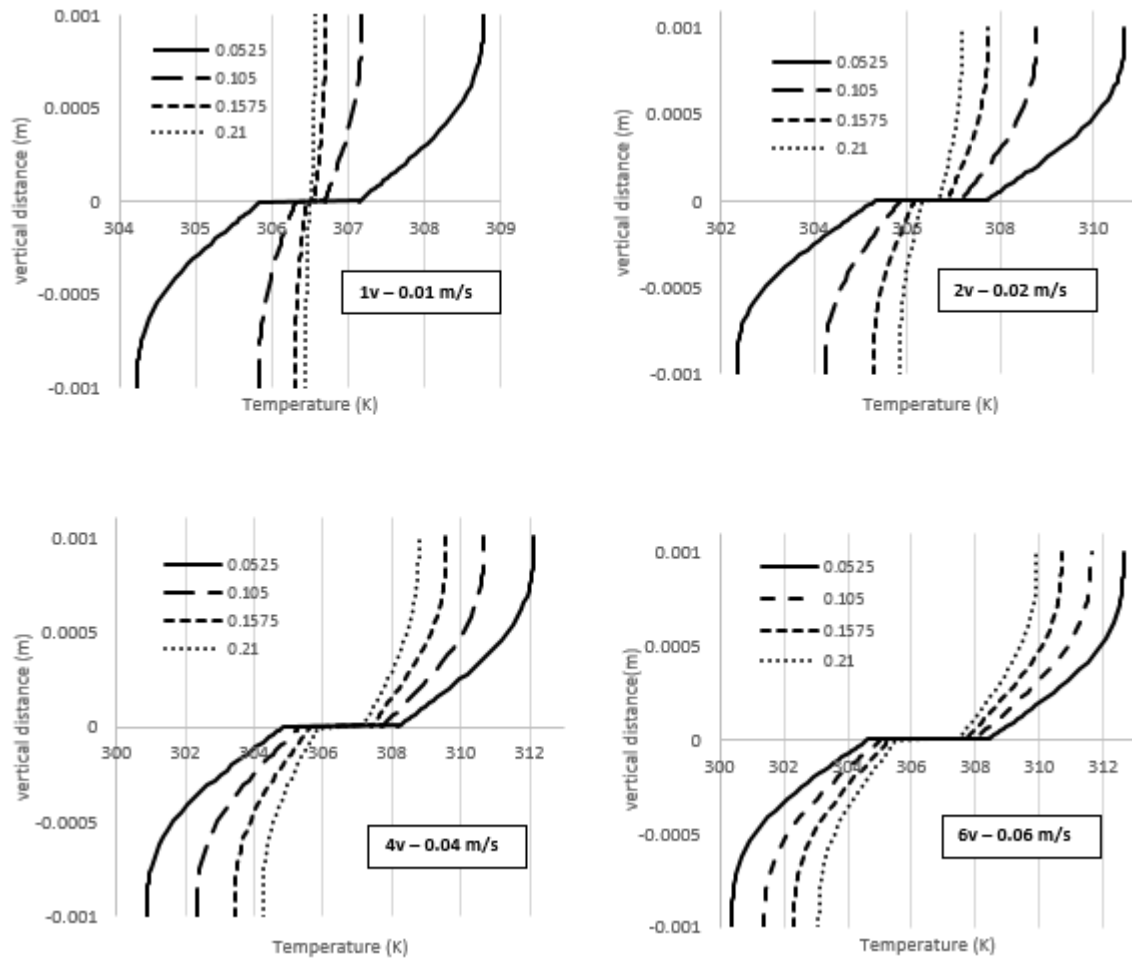
Figure 9. Temperature distributions for velocities 1v-4v across the DCMD setup

Figure 9 displays the temperature profiles across the upper and lower channels of the DCMD. The temperatures in the positive axis represent the feed side, while the temperatures in the negative axis represent the permeate side. These results were obtained as a function of the vertical distance that is the height of the channels (1mm each). The four temperature profiles in each graph represent four points along the horizontal distance chosen randomly, which are 0.0525, 0.105, 0.1575, and 0.21. These graphs indicate that by increasing velocity from 1v to 4v, the temperature trend gets closer at all points along the channel. Moreover, with higher velocity 6v, temperatures tend to increase. For example, at 6v, at point 0.0525, the temperatures are higher at the feed side and lower at the permeate side in comparison with velocity 4v graph. Also, with higher velocity, the temperature range across the membrane is higher, indicating that most of the heat transfer occurs within the membrane.

Parametric Analysis

To complement the above analysis, a parametric analysis was performed to identify the possible effects of varying the geometry of the DCMD on its performance.

Horizontal Distance

This study involved altering the horizontal distance of the channels to examine the impact. A number of simulations were run to study the effect of varying the horizontal distance. Therefore, six cases of length were chosen for four velocities (shown in Table 3 below), where the mass flow and average temperature polarization were determined.

Table 3. Horizontal distances and velocity

Horizontal length	m	Velocity	m/s
0.5x	0.105	1v	0.01
0.75x	0.1575	2v	0.02
1x	0.21	4v	0.04
2x	0.42	6v	0.06
4x	0.84		
6x	1.26		

Figure 10 consists of two graphs: (a) for the effect of total accumulative mass flow and (b) for the average temperature polarization for varying length and velocity. It can be noticed, a higher mass flux is achieved with higher velocity; the highest reported is above 4 kg/m^2.hr. Also, the accumulative mass flow slowly increases for increased horizontal distance. That is, for velocity v and 2v, the mass flux is barely increasing from 0.5x to 6x. For a higher velocity. 6v, increasing the length from 0.5x to 6x can result in an increase of almost 3 kg/m^2.hr, which is quit noticeable. This study helps determine and optimize the performance of the DCMD, keeping in mind the cost effectiveness of the DCMD geometry. On the right, Figure 10b displays the temperature polarization as a function of velocity and distance. Generally, the trend is of a decreasing nature, as the heat is lost and therefore minimal temperature exchange occurs, as the flow tends to reach the exit. However, lower
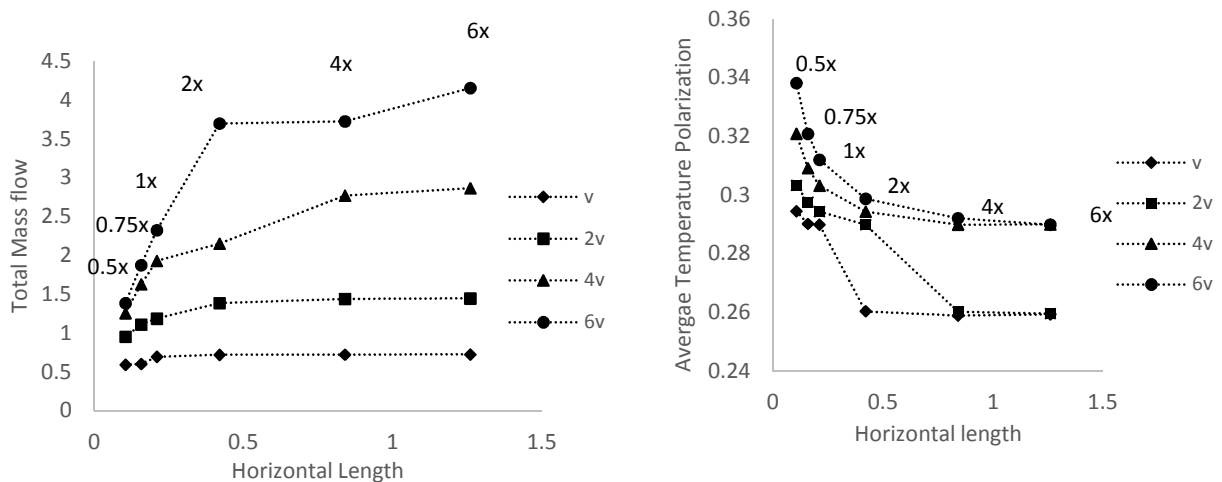

Figure 10. a) Total mass flow rate vs velocity for different horizontal channel length; b) average temperature polarization

velocity v is associated with a higher temperature polarization in comparison with velocity 6; this, in turn, tells us that higher velocity triggers unnecessary frictional flow losses.

Vertical Distance

The same study was conducted for vertical distance, keeping four velocities and four vertical lengths as listed below in Table 4.

Table 4. Vertical distances and velocity

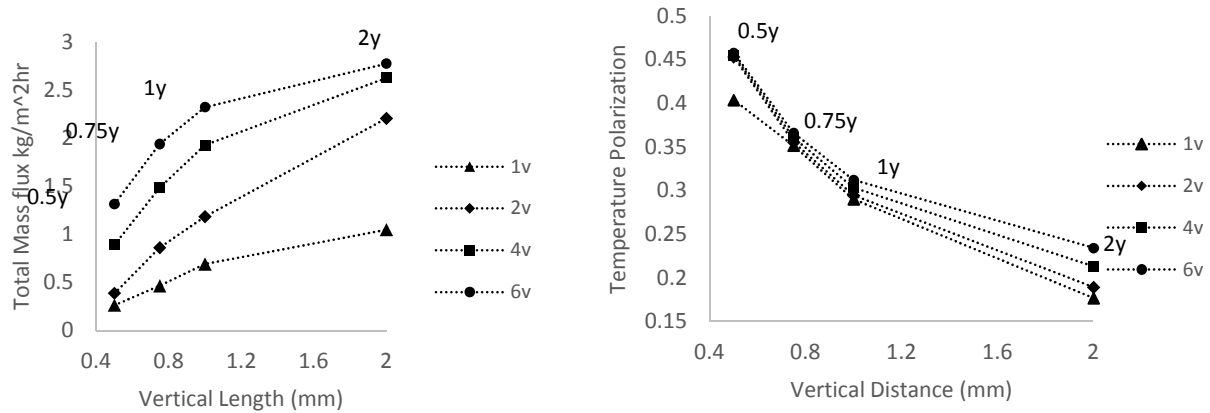| Vertical Length	mm	Velocity	m/s
0.5y	0.5	1v	0.01
0.75y	0.75	2v	0.02
1y	1	4v	0.04
2y	2	6v	0.06

Figure 11. a) Total Mass flow rate vs velocity for different vertical channel length; b) Average temperature polarization

Figure 11 represents both mass flux and temperature polarization for varying vertical distances and velocities. For the mass flux, the increasing trend is similar to the trend spotted for the horizontal study. However, for velocity 6, a higher mass flux was achieved with the horizontal study at 6x than the vertical study at 2y. In addition, there is a marginal increase with every vertical distance studied; unlike with the horizontal study, extreme distances like 6x resulted in higher flux. For the temperature polarization, it seems that it is less affected by the velocity in comparison with the polarization ratios in the horizontal study. However, it is worth noting that the decrease in temperature polarization is linear and drastic by increasing the vertical distance, while the horizontal distance suffered a lower decrease.

Conclusions

Conjugate heat computational fluid dynamics was applied to determine a high-fidelity analysis for the DCMD. The model evaluates and returns the bulk temperature and membrane temperature at the two sides of the two parallel flow representing the hot feed and cooler permeate. The temperature gradient across the membrane creates a difference in the saturation pressure across the membrane fluid, which drives mass and energy transfer through the membrane from the feed to the permeate side. The model is utilized to investigate local and accumulative flow parameters, including mass flux, heat flux, and DCMD metrics. The increase in the inlet flow resulted in a higher values of mass flux this is due to the higher convective heat flux as illustrated by the higher values of the Nusselt number. Temperature polarization was investigated. Beyond the entry region, neither heat nor mass transfer limitation occurs as the TP values remains within the allotted values (0.2, 0.6). In view of these results, the efficiency of the process is evaluated and found to be extremely low for once through. Therefore, a detailed sensitivity analysis is suggested to find the optimal yield and process metrics.

Lastly, the parametric study reflected that velocity change could produce pronounced effects on both the mass flux and temperature polarization. Also, the highest mass flux achieved above 4 kg/m^2.hr and was in the horizontal study at velocity 6v and 6x. However, drawing quantitative conclusions on whether to vary the horizontal or vertical distance will need a more in-depth case study and will be implemented in the near future.

Acknowledgments

References

[1]   Greenlee, L. F., Lawler, D. F., Freeman, B. D., Marrot, B., & Moulin, P. (2009). Reverse Osmosis Desalination: Water Sources, Technology, and Today's Challenges. *Water Research*, *43*(9), 2317-2348.
[2]   Lawson, K. W., & Lloyd, D. R. (1996). Membrane Distillation. II. Direct Contact MD, *Journal of Membrane Science*, *120*(1), 123-133.
[3]   Chen, T., & Ho, C. (2010). Immediate Assisted Solar Direct Contact Membrane Distillation in Saline Water Desalination. *Journal of Membrane Science*, *358*(1-2), 122-130.
[4]   Khayet, M., & Matsuura, T. (2011). *Membrane Distillation, Principles and Applications*. Amsterdam: Elseveier.
[5]   de Andrés, M. C., Doria, J., Khayet, M., Peña, L., & Mengual, J. J. (1998). Coupling of a Membrane Distillation Module to a Multieffect Distiller for Pure Water Production. *Desalination*, *115*(1), 71-81.
[6]   Yu, H., Yang, X., Wang, R., & Fane, A. G. (2011). Numerical Simulation of Heat and Mass Transfer in Direct Membrane Distillation in a Hollow Fiber Module with Laminar Flow. *Journal of Membrane Science*, *384*(1-2), 107-116.

[7] Zhang, L.-Z., Liang, C.-H., & Pei, L.-X. (2010). Conjugate Heat and Mass Transfer in Membrane-Formed Channels in All Entry Regions. *International Journal of Heat Mass Transfer*, *53*(5-6), 815-824.

[8] Gryta, M., & Tomaszewska, M. (1998). Heat Transport in the Membrane Distillation Process. *Journal of Membrane Science*, *144*(1-2), 211-222.

[9] Aravinth, S. (2000). Prediction of Heat and Mass Transfer for Fully Developed Turbulent Fluid Flow through Tubes. *International Joural of Heat Mass Transfer*, *43*(8), 1399-1408.

[10] Qtaishat, M., Matsuura, T., Kruczek, B., & Khayet, M. (2008). Heat and Mass Transfer Analysis in Direct Contact Membrane Distillation. *Desalination*, *219*(1-3), 272-292.

[11] Zhang, L.-Z. (2010). Heat and Mass Transfer in a Quasi-Counter Flow Membrane-Based Total Heat Exchanger. *International Journal of Heat Mass Transfer*, *53*(23-24), 5478-5486.

[12] Phattaranawik, J., Jiraratananon, R., & Fane, A. G. (2003). Heat Transport and Membrane Distillation Coefficients in Direct Contact Membrane Distillation. *Journal of Membrane Science*, *212*(1-2), 177-193.

[13] Schofield, R. W., Fane, A. G., & Fell, C. J. D. (1987). Heat and Mass Transfer in Membrane Distillation. *Journal of Membrane Science*, *33*(3), 299-313.

[14] Janajreh, I., Suwwan, D., & Faith, H. (2014). Flow Analysis of Low Energy Direct Contact Membrane Desalination. *International Journal of Thermal & Environmental Engineering*, *8*(2), 133-138.

[15] Charfi, K., Khayet, M., & Safi, M. J. (2010). Numerical Simulation and Experimental Studies on Heat and Mass Transfer Using Sweeping Gas Membrane Distillation. *Desalination*, *259*(1-3), 84-96.

[16] Termpiyakul, P., Jiraratananon, R., & Srisurichan, S. (2009). Heat and Mass Transfer Characteristics of a Direct Contact Membrane Distillation Process for Desalination. *Desalination*, *177*(1-2), 133-141.

[17] Chen, T.-C., Ho, C.-D., & Yeh, H.-M. (2009). Theoretical Modeling and Experimental Analysis of Direct Contact Membrane Distillation. *Journal of Membrane Science*, *330*(1-2), 297-287.

[18] Zhongwei, D., Liu, L., El-Bourawi, M. S., & Runyu, M. (2005). Analysis of a Solar-Powered Membrane Distillation System, *Desalination*, *172*(1), 27-40.

[19] Bui, V. A., Vu, L. T. T., & Nguyen, M. H. (2010). Modelling the Simultaneous Heat and mass transfer of Direct Contact Membrane Distillation in Hollow Fibre Modules. *Journal of Membrane Science*, *353*(1–2), 85–93.

[20] Imdakm, A. O., & Matsuura, T. (2005). Simulation of Heat and Mass Transfer in Direct Contact Membrane Distillation (MD): The Effect of Membrane Physical Properties. *Journal of Membrane Science*, *262*(1-2), 117-128.

[21] Iversen, S. B., Bhatia, V. K., Dam-Johansen, K., & Jonsson, G. (1997). Characterization of Microporous Membranes for Use in Membrane Contactors. *Journal of Membrane Science*, *130*(1-2), 205-217.

[22] Gryta, M., Tomaszewska, M., & Morawski, A. W. (1997). Membrane Distillation with Laminar Flow. *Separation and Purification Technology*, *11*(2), 93-101.

Biographies

ISAM JANAJREH received his PhD and master's from Virginia Tech in Engineering Science and Mechanics and Mechanical Engineering respectively. He received his BS in Mechanical Engineering from Jordan University of Science and Technology. Dr. Janajreh's focus was on solid-fluid interactions, turbulence modeling and mixing, and thermo mechanical coupling. He was visiting professor at Virginia Tech at the Engineering Science and Mechanics and Math Departments through 1998 and later joined Michelin R&D, USA, as a tire and automotive research engineer, analyzing wet tire traction and nonlinear structure analysis, vehicle dynamics, and rubber material modeling. Dr. Janajreh joined Masdar in 2007 continuing his research while also teaching advanced renewable energy conversion system, fundamentals of combustion, advanced fluid dynamics, and computational fluid dynamics. He has authored over 15 referenced publications on fluid dynamics and structure interaction, made more than 35 contributions to international conferences and is a key contributor to three Michelin patents (Catamaran, Primacy, X-one)and three books (traction, rolling, resistance noise). Dr. Janajreh can be reached at ijanajreh@masdar.ac.ae.

DANA SUWWAN is a master's student and a research assistant in her first year in Waste to Energy Lab at Masdar Institute of Science and Technology. Her interests lie within developing a full-fledged study on the possible ways to enhance the productivity of the DCMD, be it energy-wise or on a molecular development level. Dana can be reached at dsuwwan@masdar.ac.ae.